

Exploring Satellite-Derived Relationships between Cloud Droplet Number Concentration and Liquid Water Path Using a Large-Domain Large-Eddy Simulation



Tellus B

Chemical and Physical Meteorology

ORIGINAL RESEARCH
PAPER

SUDHAKAR DIPU

MATTHIAS SCHWARZ

ANNICA M. L. EKMAN

EDWARD GRYSPEERDT

TOM GOREN

ODRAN SOURDEVAL

JOHANNES MÜLMENSTÄDT

JOHANNES QUAAS

*Author affiliations can be found in the back matter of this article



STOCKHOLM
UNIVERSITY PRESS

ABSTRACT

Important aspects of the adjustments to aerosol-cloud interactions can be examined using the relationship between cloud droplet number concentration (N_d) and liquid water path (LWP). Specifically, this relation can constrain the role of aerosols in leading to thicker or thinner clouds in response to adjustment mechanisms. This study investigates the satellite retrieved relationship between N_d and LWP for a selected case of mid-latitude continental clouds using high-resolution Large-eddy simulations (LES) over a large domain in weather prediction mode. Since the satellite retrieval uses the adiabatic assumption to derive the N_d , we have also considered adiabatic N_d (N_{Ad}) from the LES model for comparison. The joint histogram analysis shows that the N_{Ad} -LWP relationship in the LES model and the satellite is in approximate agreement. In both cases, the peak conditional probability (CP) is confined to lower N_{Ad} and LWP; the corresponding mean LWP (\overline{LWP}) shows a weak relation with N_{Ad} . The CP shows a larger spread at higher N_{Ad} ($>50 \text{ cm}^{-3}$), and the LWP increases non-monotonically with increasing N_{Ad} in both cases. Nevertheless, both lack the negative N_{Ad} -LWP relationship at higher N_{Ad} , the entrainment effect on cloud droplets. In contrast, the model simulated N_d -LWP clearly illustrates a much more nonlinear (an increase in LWP with increasing N_d and a decrease in LWP at higher N_d) relationship, which clearly depicts the cloud lifetime and the entrainment effect. Additionally, our analysis demonstrates a regime dependency (marine and continental) in the N_{Ad} -LWP relation from the satellite retrievals. Comparing local vs large-scale statistics from satellite data shows that continental clouds exhibit only a weak nonlinear N_{Ad} -LWP relationship. Hence a regime-based N_d -LWP analysis is even more relevant when it comes to warm continental clouds and their comparison to satellite retrievals.

CORRESPONDING AUTHOR:

Sudhakar Dipu

Institute for Meteorology,
Universität Leipzig, Leipzig,
Germany

dipu.sudhakar@uni-leipzig.de

KEYWORDS:

Aerosol-cloud interaction; Cloud droplet number concentration; Liquid water path

TO CITE THIS ARTICLE:

Dipu, S, Schwarz, M, Ekman, AML, Gryspeerdt, E, Goren, T, Sourdeval, O, Mülmenstädt, J and Quaas, J. 2022. Exploring Satellite-Derived Relationships between Cloud Droplet Number Concentration and Liquid Water Path Using a Large-Domain Large-Eddy Simulation. *Tellus B: Chemical and Physical Meteorology*, 74(2022):176–188. DOI: <https://doi.org/10.16993/tellusb.27>

1. INTRODUCTION

Clouds play a remarkable role in the Earth's radiation budget (Ramanathan et al., 1989). Cloud properties are modulated by atmospheric aerosols, as almost all the liquid cloud droplets form on an aerosol particle that can act as cloud condensation nuclei (Charlson et al., 1992; Twomey, 1974). Twomey (1974) hypothesized that an aerosol perturbation could modify the cloud droplet number concentration (N_d), which enhances the cloud albedo (now commonly referred to as the radiative forcing due to aerosol-cloud interactions, RF_{ACI} Bellouin et al., 2020; Forster et al., 2021). At higher N_d , precipitation formation via collision-coalescence is slowed down or suppressed, implying a possible increase in the liquid water path (LWP) (Albrecht, 1989). Numerous further mechanisms, known as rapid adjustments to aerosol-cloud interactions (summarized, e.g., by Gryspeerdt et al., 2019), may lead to enhancements or decreases in LWP at larger N_d . Recent studies reveal that the time-dependency of these adjustment processes is crucial (Christensen et al., 2020; Gryspeerdt et al., 2021; Glassmeier et al., 2021). Besides their impact on LWP, adjustment mechanisms may also influence horizontal cloud extent (Gryspeerdt et al., 2016) or cloud-top temperatures (Rosenfeld et al., 2014; Bellouin et al., 2020). The combination of the radiative forcing due to the aerosol-cloud interactions, and these adjustments, is known as the effective radiative forcing due to aerosol-cloud interactions, ERF_{ACI} . Still, ERF_{ACI} constitutes the largest uncertainty among all forcing agents (Mülmenstädt & Feingold, 2018; Chen et al., 2014; Rosenfeld et al., 2014; Forster et al., 2021; Szopa et al., 2021).

Satellite observations play a crucial role in understanding and quantifying the RF_{ACI} (a component of effective radiative forcing, ERF_{ACI}) globally (Stephens et al., 2019) and in evaluating aerosol-cloud interactions in climate models (Saponaro et al., 2020). However, large uncertainties remain in satellite-based aerosol-cloud interaction estimates. This stems from retrieval artefacts in satellite products, asynchronous retrieval of aerosol and cloud properties, and limited abilities to observe the relevant processes (Stevens & Feingold, 2009; Christensen et al., 2017; Grosvenor et al., 2018; Quaas et al., 2020; Jia et al., 2021). Nevertheless, the co-variation in aerosol and cloud optical properties has been used to estimate aerosol-cloud interactions and, consequently, the RF_{ACI} (Feingold et al., 2003; Quaas et al., 2008; McCoy et al., 2017; Hasekamp et al., 2019). Recent studies proposed that the relationship between N_d and LWP is a vital metric for estimating the LWP adjustment to aerosol-cloud interactions (Gryspeerdt et al., 2019; Bulatovic et al., 2019). The relationship between N_d and LWP could constrain the role of the aerosols in adjustments to aerosol-cloud interactions if combined

with an estimate of the anthropogenic perturbation to N_d (Michibata et al., 2016; Bellouin et al., 2020). Gryspeerdt et al. (2019) analyzed in much detail the relationship between satellite-derived N_d and LWP. They found that the N_d -LWP relationship is highly nonlinear over the Global Oceans, indicating that the LWP increases for lower N_d and the LWP decreases for higher N_d . A positive N_d -LWP relationship could result from precipitation formation delay or suppression (Albrecht, 1989; Suzuki et al., 2013). Also, warm cloud invigoration can lead to positive N_d -LWP relations (Koren et al., 2014). On the contrary, a negative N_d -LWP relationship may indicate an impact of cloud entrainment and mixing (Ackerman et al., 2004; Chen et al., 2014; Xue & Feingold, 2006; Michibata et al., 2016; Sato et al., 2018). A positive N_d -LWP sensitivity may, in turn, imply a negative contribution to ERF_{ACI} (additional cooling effect), while negative ones result in a positive (warming) contribution (Toll et al., 2019; Bellouin et al., 2020).

Although N_d is a crucial parameter for understanding aerosol-cloud interactions, none of the standard satellite retrieval algorithms directly provide this variable. A common method uses the cloud optical thickness and effective radius from passive satellite observations to infer N_d (Quaas et al., 2006). The satellite retrieved N_d is based on the adiabatic assumption, where N_d is assumed to be constant with height and the cloud liquid water content is assumed to increase linearly with height (Brennguier et al., 2000; Schüller et al., 2005). Applying these assumptions in satellite-based analysis reveals a negative RF_{ACI} (Twomey effect, a positive N_d -LWP sensitivity), which is partially offset by the LWP adjustment (negative N_d -LWP sensitivity) due to aerosol-cloud interaction (Toll et al., 2019). The magnitude and even sign of this LWP adjustment are very uncertain; this generates uncertainty in ERF_{ACI} (Forster et al., 2021). However, the adiabatic assumption and the satellite retrievals of cloud optical thickness and effective radius are uncertain (Grosvenor et al., 2018; Quaas et al., 2020), which also propagates to significant uncertainties in estimates of ERF_{ACI} .

This study investigates assumptions made to evaluate the N_d -LWP relationships from satellite observations by using the results of a large-domain large-eddy simulation. The idea is that a comparison of the N_d -LWP relationship between a high-resolution model and satellite retrieval allows an understanding of the impacts of biases and assumptions used in the satellite N_d and LWP retrievals.

2. DATA AND METHODOLOGY

2.1. THE ICON-LES SIMULATION

In this study, we have analyzed available Large-eddy simulations (LES) using the ICOSahedral Nonhydrostatic (ICON) model (Dipankar et al., 2015; Zängl et al., 2015).

The atmospheric model ICON is a unified model for numerical weather prediction and climate simulations. As an extension, Dipankar et al. (2015) configured the ICON to a large-eddy simulation framework, which has been validated against standard LES models and data (Heinze et al., 2017). Here, we have used the available ICON-LES simulation from the High Definition Clouds and Precipitation for advancing Climate Prediction (HD(CP)²) project. The simulation was carried out over a large domain over Germany in a weather prediction mode with realistic boundary conditions from the operational COSMOS-DE (Consortium for Small Scale Modelling, Baldauf et al., 2011), including a fully interactive land surface (Costa-Surós et al., 2020). The simulation was performed with a horizontal resolution of 156 m and 150 vertical levels with a model top at 21 km. Near the surface, the minimum layer thickness is 20 m, and the lowest 1000 m confines 20 layers (Heinze et al., 2017). The ICON-LES uses a new sub-grid scale turbulence scheme based on the classical Smagorinsky scheme, which also accounts for thermal stratification (Lilly, 1962). The LES uses a detailed two-moment liquid and ice-phase cloud micro-physics scheme implemented by Seifert & Beheng (2006). The Sommeria & Deardorff (1977) cloud fraction scheme assumes that within the grid box, the cloud fraction is either 1 or 0. CCN concentrations are prescribed in the study as a temporally and spatially varying distribution for the years 2013 and (at much larger pollution levels) 1985 (Costa-Surós et al., 2020). For this study, we have selected the simulation performed for 2 May 2013. It has been one of the extensive measurement campaigns for HD(CP)² Observational Prototype Experiment (HOPE, Löhnert et al., 2015; Madhavan et al., 2016). A detailed description of the ICON-LES model and HD(CP)² simulation can be obtained from Dipankar et al. (2015), Heinze et al. (2017), and Costa-Surós et al. (2020).

The respective date of the study has been selected based on the evaluation results from Heinze et al. (2017) as a case in which a wide range of cloud regimes was present. Heinze et al. (2017) reported that the ICON-LES clouds are well represented compared to the satellite observations. They found a very good agreement between simulated cloud water paths and satellite retrievals. A slight underestimation in cloud fraction was observed, though. Additionally, the simulated vertical cloud profiles are in accordance with the satellite observations. Furthermore, Costa-Surós et al. (2020) documented that the LWP from the model and the satellite compare well. They also revealed that the simulated cloud profiles (effective radius, droplet number and liquid water content) are consistent with the ground-based observations. The above studies suggest that the simulated cloud micro-physical properties are consistent with both satellite and ground-based observations. Hence, the specific case simulated by the ICON-LES is

conclusive for aerosol interaction studies and comparing it with the satellite analysis.

Although the ICON-LES simulation is performed with 156 m horizontal resolution, in our analysis, we have used coarse gridded data with a resolution of 1.2 km (grid size of 589 × 637) to approximately match the resolution of the satellite retrievals. The cloud-top is defined as the topmost level of the cloudy grid point with $N_d > 2 \text{ cm}^{-3}$. The corresponding cloud-top N_d are extracted for single-layered non-precipitating liquid clouds from the model. For the analysis, the cloud-top N_d is filtered for cloud fractions equal to 1 (at the 1.2 km scale) and cloud optical thicknesses greater than 2. To restrict the analysis to liquid clouds, we excluded the clouds with a cloud-top temperature of less than 268 K. Further, to avoid fog, cloud base heights greater than 300 m were selected for the analysis. For the chosen clouds, adiabatic cloud droplet number concentration (N_{Ad}) is calculated from cloud-top effective radius and cloud optical thickness using the relation suggested by Quaas et al. (2006). The cloud parameters are further filtered for the updraft regions and the cloud cores by choosing grid boxes with a positive vertical velocity ($w > 0$) and relative humidity greater than 100% (Heiblum et al., 2019). For the cloud regime classification, clouds with thicknesses between 100 to 600 m are considered shallow clouds; those with thicknesses greater than 1000 m are convective clouds. For the joint histogram analysis, hourly instantaneous model output from 0800 hrs to 2000 hrs is considered, and the corresponding data is compared with the satellite observation.

2.2. SATELLITE DATA

We use cloud optical properties from the Moderate Resolution Imaging Spectroradiometer (MODIS, Platnick et al., 2017) onboard the Aqua satellite. The cloud properties are obtained from MODIS Level2 collection 6.1 (MYDO6_L2) at 1 km × 1 km resolution (Menzel et al., 2015). The cloud droplet number concentration (N_{Ad}) is retrieved from cloud optical thickness and effective radius from this data set, which uses the adiabatic assumption (Quaas et al., 2006; Gryspeerdt et al., 2019). The N_{Ad} is then filtered for single-layer liquid clouds with a cloud-top temperature greater than 268 K and pixels with a cloud fraction greater than 0.9. Additionally, the cloud optical depth of less than two is excluded from the analysis (Gryspeerdt et al., 2019; Bennartz & Rausch, 2017; Grosvenor & Wood, 2014). The MODIS Level2 cloud fraction with 5 km resolution has been interpolated to 1 km by 1 km and used in the analysis. For the Northern hemispheric (0°N to 90°N) and the global analysis, cloud products from both MODIS Level2 and Level3 data sets are used. The MODIS Level3 (MYD08_D3) data from the period 2003–2020 and MODIS Level2 data from the period 2013–2017 are used.

Hereafter, N_d stands for the cloud droplet number concentration at the cloud-top (diagnosed in the model). Similarly, N_{Ad} indicates adiabatic cloud droplet number concentration (considered vertically uniform; from both model and satellite retrievals). The joint histograms analyzed in this study are constructed as conditional probabilities (CP [%]) following Gryspeerdt et al. (2016) and are defined as the probability of finding a certain LWP given that a certain N_d has been observed (CP = [P(LWP| N_d) × 100]). For the joint histogram analysis, 20 bins are used with varying sampling data in each bin. In the following text, the nonlinear relation implies that both negative and positive N_d/N_{Ad} -LWP sensitivities (positive and negative relation) coexist.

3. RESULTS

3.1. CLOUD REGIME WITH THE ADIABATIC ASSUMPTION

The sensitivity in N_{Ad} to LWP is investigated using a joint probability histogram analysis as described by Gryspeerdt et al. (2016). Figure 1 shows the comparison between the ICON-LES and satellite-derived N_{Ad} -LWP joint histograms over Germany. In both the model and the satellite, the peak (narrowest) CP is confined to the lower N_{Ad} (<100 cm^{-3}). At these lower N_{Ad} , the model shows the peak CP is distributed between the LWP 30 and 60 g m^{-2} , with no clear relation between N_{Ad} and LWP (Figure 1a). The satellite data, however, suggests that there is a high probability of observing a decreasing LWP with increasing N_{Ad} at these low N_{Ad} values (Figure 1b). For higher N_{Ad} (>100 cm^{-3}), both the model and the satellite show a larger CP spread, with a tendency to increase LWP

as N_{Ad} increases. In the joint histogram, the change of the mean LWP ($\overline{\text{LWP}}$) with N_{Ad} generally reflects the tendency of the N_{Ad} -LWP relation. For the ICON-LES, $\overline{\text{LWP}}$ slightly increases with increasing N_{Ad} at lower values ($N_{Ad} < 100 \text{ cm}^{-3}$) and then it increases sharply until $N_{Ad} \approx 300 \text{ cm}^{-3}$. Further, the $\overline{\text{LWP}}$ shows a slight increase with increasing N_{Ad} (Figure 1a). In the case of the satellite-derived joint histogram, the $\overline{\text{LWP}}$ shows a slight decrease with increasing N_{Ad} instead of an increase compared to the model, and it almost follows the peak CP. For higher N_{Ad} (>100 cm^{-3}), the $\overline{\text{LWP}}$ increases non-linearly with increasing N_{Ad} (Figure 1b). In both the model and the satellite, the selected continental boreal spring case (2 May 2013), the N_{Ad} -LWP relationship is positive and nonlinear; however, the relationship lacks, in particular, the negative relationship at higher N_{Ad} (where it is hypothesized that more entrainment at larger droplet concentrations may lead to depletion of LWP). However, Gryspeerdt et al. (2019) reported a highly nonlinear N_{Ad} -LWP sensitivity with increasing LWP at low N_{Ad} and decreasing LWP at high N_{Ad} over the Global Oceans using satellite data.

The regime dependence of the N_{Ad} -LWP relationship and the representativeness of the particular case available for the joint satellite-LES analysis are further analyzed using MODIS satellite retrievals (Figure 2). Using the MODIS Level2, the N_{Ad} -LWP relationship over the Northern Hemisphere (NH) Land for the selected ICON-LES simulation date (2 May 2013) is illustrated in Figure 2a. The figure shows that the satellite retrieved N_{Ad} -LWP relationship over NH Land is very similar to that of the LWP- N_{Ad} relationship over Germany (Figure 1b). In both cases, for the lower N_{Ad} (<100 cm^{-3}), the peak CP appears along the lower LWP as N_{Ad} increases, despite

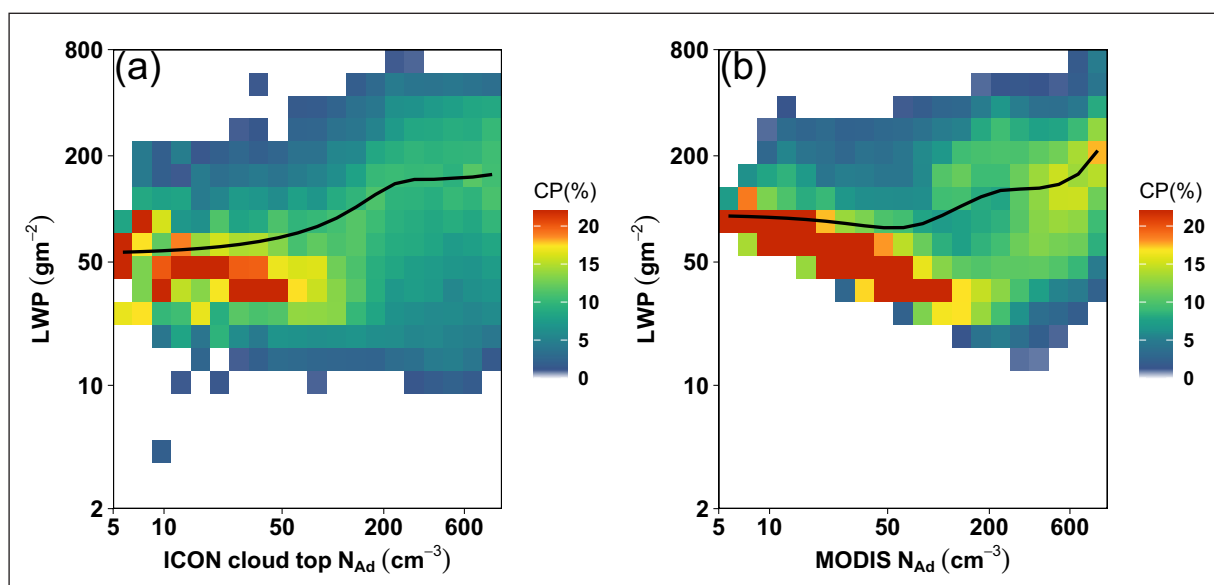


Figure 1 The N_{Ad} -LWP joint histogram in (a) the ICON-LES model, and (b) the MODIS-Level2 satellite retrieval, over Germany. The thick black line in each plot shows the mean LWP (LWP) at certain N_d bins (P(LWP| N_d)). CP(%) is condition probability: the probability of finding a certain LWP given that a certain N_d has been observed.

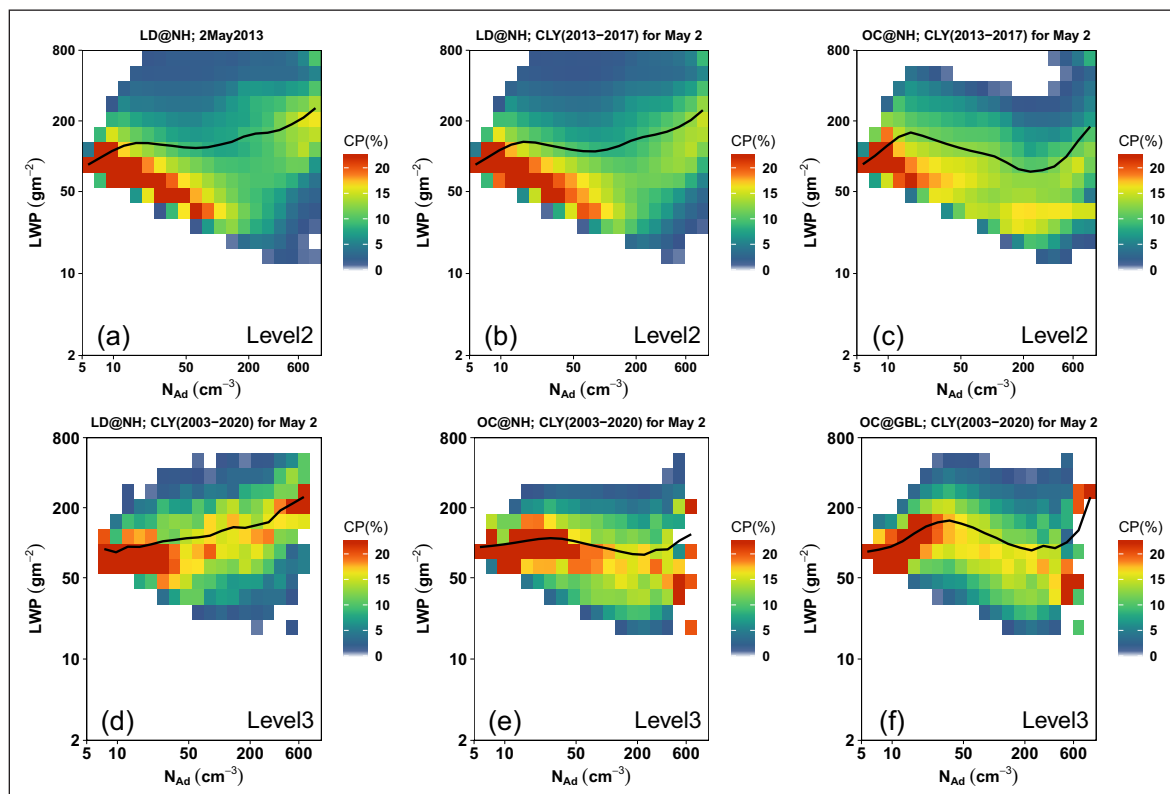


Figure 2 The N_{Ad} -LWP joint histogram for (a) the Northern hemisphere Land for the date 02 May 2013 using MODIS-Level2, (b) daily climatology (02 May 2013) for the Northern hemisphere Land for the period 2013–2017 using MODIS-Level2, (c) same as fig (b) but for the Northern hemisphere Ocean using MODIS-Level2, (d) daily climatology (02 May 2013) for the Northern hemisphere Land for the period 2003–2020 using MODIS-Level3, (e) same as fig (d) but for the Northern hemisphere Ocean using MODIS-Level3, and (f) daily climatology (02 May 2013) for the Global Ocean using MODIS-Level3. The figure description is the same as Figure 1.

the NH Land showing a nonlinear pattern in \overline{LWP} (slight increase and decrease), especially at the lower N_{Ad} ($N_{Ad} < 100 \text{ cm}^{-3}$). Also, both cases show that the \overline{LWP} increases with increasing N_{Ad} (after the $N_{Ad} > 100 \text{ cm}^{-3}$). Further, the 2 May multi-year statistic of the N_{Ad} -LWP relationship over the NH Land (Figure 2b) is analogous to both relationships for the specific date over Germany and the NH Land. The N_{Ad} -LWP relationship over the NH Land, both for the selected day and the multi-year statistics, illustrates a similar relationship that persists irrespective of the sampling area and the period in spite of the diverse cloud pattern for the respective area/years. It lends credibility to the geographical representativeness of the evaluation between the satellite and the LES for the particular case. However, over the NH Ocean (the N_{Ad} -LWP climatology), the peak CP is more or less confined to the \overline{LWP} (Figure 2c). For low N_{Ad} ($< 20 \text{ cm}^{-3}$), the peak CP appears along with increasing \overline{LWP} as the N_{Ad} increases. Beyond 20 cm^{-3} , as the N_{Ad} increases, the higher CP is confined along decreasing \overline{LWP} until N_{Ad} is close to 500 cm^{-3} . Finally, for the higher N_{Ad} , the CP shows a large spread between the LWP 10 and 800 gm^{-2} . Over the NH Ocean, both CP and the \overline{LWP} show a nonlinear pattern; in particular, the \overline{LWP} shows positive and negative sensitivity with N_{Ad} compared to the continental case.

In order to compare to published results (e.g., Gryspeerd et al., 2019), we have assessed the

relationships at aggregate, $1^\circ \times 1^\circ$ scales corresponding to the scale of the MODIS Level3 products. The analysis is thus repeated with MODIS Level3 data. From this aggregated data, over the NH Land for the years 2003–2020, the N_{Ad} -LWP relationship is illustrated in Figure 2d. It also shows that the peak (narrowest) CP is bound to lower N_{Ad} , and then it appears along the increasing \overline{LWP} with increasing N_{Ad} . The \overline{LWP} also follows the high CP, showing more or less a linear positive relation with N_{Ad} . When it comes to the NH Oceans, the peak CP is found at the lower N_{Ad} , similar to the NH Land, but for high N_{Ad} ($< 50 \text{ cm}^{-3}$), the high CP appears mainly along the negative N_{Ad} -LWP slope (Figure 2e). Over the NH ocean, the Level3 N_{Ad} -LWP relationship is found to resemble the Level2 result but is less pronounced. Finally, over the Global Oceans, similar to the previous cases, the peak CP is bound to the lower N_{Ad} ($< 50 \text{ cm}^{-3}$), and the relatively high CP appears along with the \overline{LWP} curve (Figure 2f). Furthermore, over the Global Ocean, the \overline{LWP} firmly follows a nonlinear relationship in which the \overline{LWP} increases at lower N_{Ad} and decreases at higher N_{Ad} . Over the Ocean (Global and NH), the N_{Ad} -LWP sensitivity is more or less identical in all three cases; nevertheless, a more pronounced nonlinear sensitivity is observed in the Level3 Global Ocean. It is similar to the previous satellite analysis reported by Gryspeerd et al. (2019), even if a longer time span is considered here. The above

analysis clearly indicates that the marine clouds show a pronounced N_{Ad} -LWP sensitivity (nonlinear: increasing N_{Ad} leads to increasing/decreasing LWP at low/high N_{Ad}) irrespective of the data in contrast to continental clouds.

From the above satellite analysis of the N_{Ad} -LWP relationship, it is noticed that over the Ocean (global and NH), a highly nonlinear relationship persists. It indicates the \overline{LWP} increase with increasing N_{Ad} at low N_{Ad} , followed by a decrease in \overline{LWP} at higher N_{Ad} ; at higher N_{Ad} , the \overline{LWP} further increase (Figure 2c, e, & f). However, in continental clouds, the negative N_{Ad} -LWP sensitivity is feeble (less nonlinear) compared to the marine clouds (highly nonlinear), which illustrates the diverse N_{Ad} -LWP relation in marine and continental clouds. Furthermore, in both MODIS Level2 and Level3 analyses, it is evident that a land-ocean contrast exists in the N_{Ad} -LWP relationship. Many reasons can lead to this distinction, such as the fact that continental clouds typically have higher cloud bases and are more heterogeneous than oceanic clouds (e.g., Unglaub et al., 2020), while marine clouds are affected by ship tracks with cleaner background conditions. In the case of continental clouds, at higher N_{Ad} , the N_{Ad} -LWP relations lack negative sensitivity due to the constraints in adiabatic assumption in deriving N_{Ad} . However, it persists in the marine clouds, which are highly susceptible to aerosol perturbation (significant reduction in higher LWP) compared to the continental clouds.

3.2. CLOUD REGIME WITHOUT ADIABATIC ASSUMPTION

The ICON-LES simulated N_d may, however, not follow the adiabatic assumption; N_d may vary with height above the cloud base. The N_d -LWP relationship, this time using cloud-top N_d , is depicted in Figure 3a. At lower N_d ($<100\text{ cm}^{-3}$), the CP shows a larger spread between LWP 10 and

800 gm^{-2} and the peak CP is confined to the lower LWP. At larger N_d ($>200\text{ cm}^{-3}$), the spread of the CP decreases relative to the lower N_d , and the corresponding high CP occurs along a negative N_d -LWP slope. Further, at lower N_d ($<100\text{ cm}^{-3}$), the \overline{LWP} increases with increasing N_d , and at higher N_d ($>200\text{ cm}^{-3}$), the \overline{LWP} decreases as the N_d increases. The nonlinear N_d -LWP relationship is similar to what has been reported from previous studies analyzing satellite data over global Oceans, which uses N_{Ad} though (Gryspeerd et al., 2019; Michibata et al., 2016). The discrepancies between the N_d -LWP and N_{Ad} -LWP relationship in the ICON-LES is further investigated by comparing N_d and N_{Ad} . Figure 3b shows the comparison between the model predicted N_d and model-derived N_{Ad} . The figure shows that peak CP occurs at $N_d > 100\text{ cm}^{-3}$ and at $N_{Ad} > 200\text{ cm}^{-3}$, with a significant correlation. At lower N_d , the CP shows a large spread for N_{Ad} , with less CP, which overestimates the actual droplet number concentration. The poorly correlated N_d - N_{Ad} relation indicates that sub-adiabatic clouds are common in the ICON-LES simulation. This is especially the case for clouds with low N_d .

The comparison between N_d and N_{Ad} indicates that for lower N_d , there are occasions/grids boxes where the adiabatic assumption holds, in particular for the high N_d case. In other words, there are regions within the sub-adiabatic cloud regimes with a constant N_d profile or adiabatic. Cloud adiabaticity (α), the ratio of LWP to the adiabatic LWP (LWP_{Ad} for an adiabatic cloud liquid water content (LWC), increases linearly with height), represents the adiabatic/sub-adiabatic cloud character. Clouds with α greater than 0.9, the cloud regimes are nearly adiabatic, and for α less than 0.9 implies sub-adiabatic or diluted clouds (Braun et al., 2018). Figure S1 shows the relation between cloud depth and LWP as a

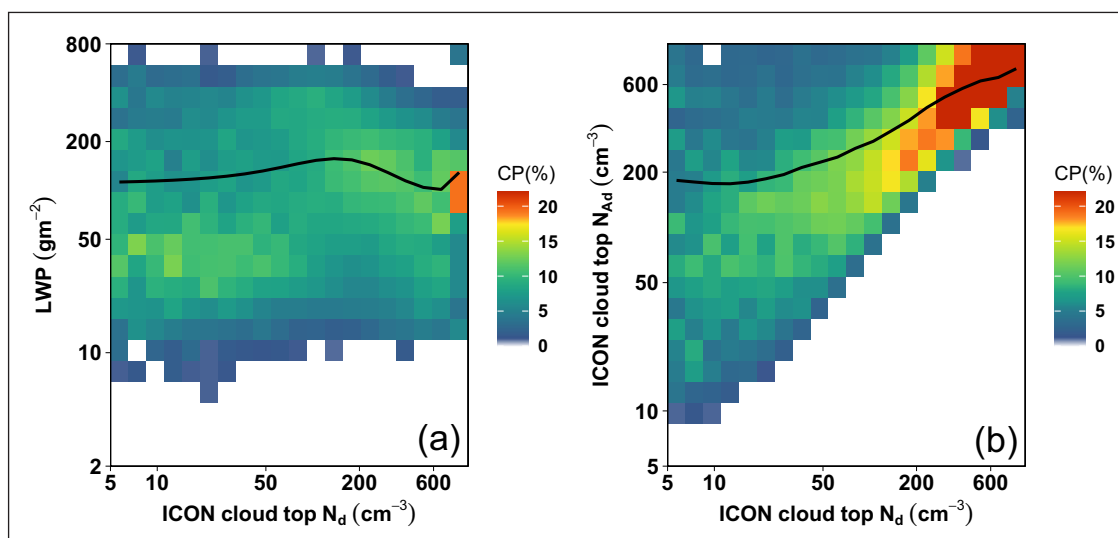


Figure 3 ICON-LES diagnostics to assess the satellite assumptions in retrieving N_d . **(a)** same as Figure 1a, but using N_d diagnosed at cloud-top, rather than N_{Ad} (over Germany), and **(b)** A comparison between model predicted N_d and model derived adiabatic N_{Ad} at the cloud-top (over Germany). The thick black line (3b) shows the mean N_{Ad} at certain N_d bins ($P(N_{Ad}|N_d)$). CP(%) is condition probability: the probability of finding a certain N_{Ad} given that a certain N_d has been observed.

function of α . The figure illustrates that the cloud LWP increases with cloud depth, and the adiabatic clouds ($\alpha \approx 1$) are confined to lower cloud depth. The highest value of α is linked to geometrically thin clouds, and the lowest value of α is associated with relatively thick clouds in the simulated continental clouds (Figure S1). It further suggests that among the continental clouds, the shallow (thin) clouds tend to be adiabatic with less entrainment and mixing, compared to convective (thick) clouds that are sub-adiabatic and associated with stronger entrainment and mixing. Figure 4 shows the mean N_d profiles of shallow and convective clouds, respectively, as diagnosed from the ICON-LES. The shallow cloud regime (depth between 100 and 600 m) shows a more or less constant mean N_d profile with height (Figure 4a), except at the very bottom and top of the clouds. These shallow clouds can thus be considered approximately adiabatic

with little lateral entrainment mixing. On the contrary, the thick convective clouds (depth greater than 1000 m) in the model have a varying mean N_d profile, within that particular decreasing N_d from the first third in cloud thickness onwards, implying a substantial mixing and sub-adiabaticity of these clouds (Figure 4b).

The N_d -LWP relationship in the adiabatic and sub-adiabatic cloud regime in the ICON-LES model (over Germany) is shown in Figure 5. In the shallow or the adiabatic cloud regime, the N_d -LWP relationship shows a positive, almost linear relationship (Figure 5a); LWP tends to increase with increasing N_d , and the peak CP occurs along the LWP. For the shallow cloud regime, the CP is mainly confined to LWP between 2 and 200 gm^{-2} . For the convective or the sub-adiabatic cloud regime, the N_d -LWP relation is nonlinear (Figure 5b). The LWP slightly increases at the lower N_d and slightly decreases

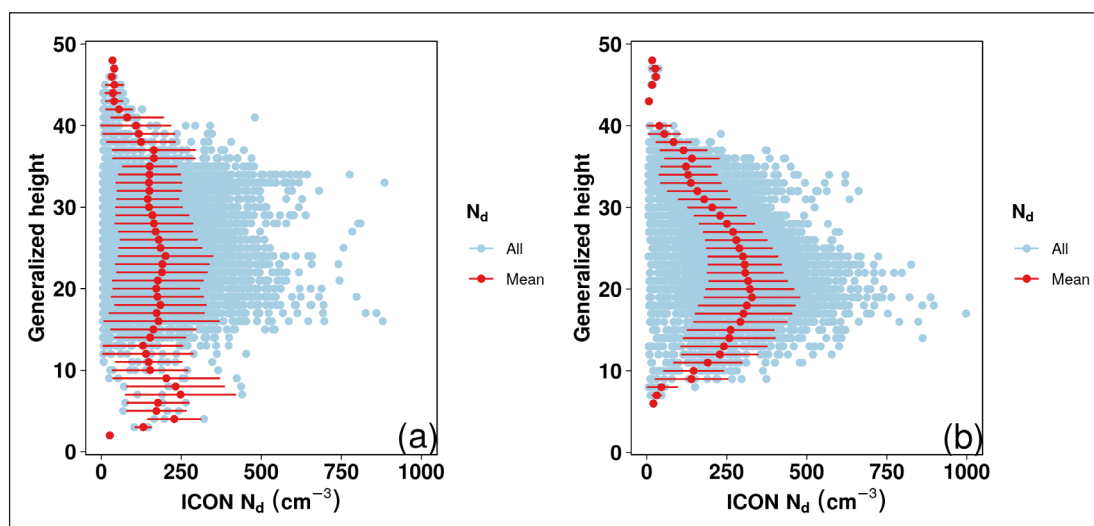


Figure 4 The ICON-LES N_d (cm^{-3}) profile (over Germany) for (a) a shallow cloud regime, and (b) a convective cloud regime. The blue points indicate individual cloud profiles for the respective model grid, and the red points indicate the mean cloud profile with standard deviations.

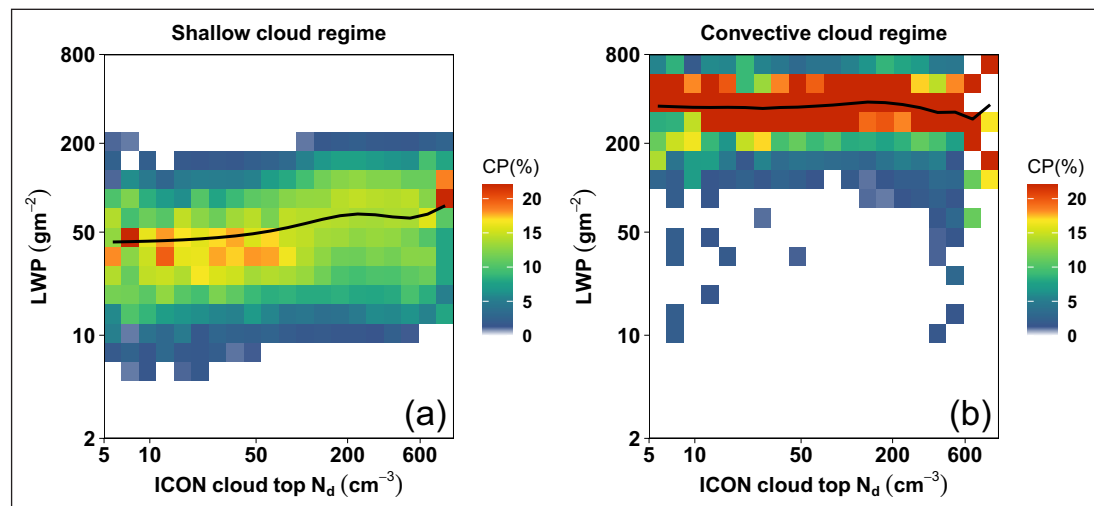


Figure 5 The N_d -LWP joint histogram (over Germany) for (a) the shallow cloud regime with the cloud depth between 100 to 600 m, and (b) the convective cloud regime with the cloud depth greater than 1000 m. The figure description is the same as Figure 1.

at the higher N_d (note the logarithmic axis). The peak CP appears for almost all N_d , and it is confined to higher LWP between 500 and 700 gm^{-2} . Compared to the adiabatic cloud regime, in the sub-adiabatic clouds, the CP ranges between 10 to 800 gm^{-2} LWP. However, the sub-adiabatic N_d -LWP relationship is comparable to the ICON-LES simulated N_d -LWP relationship.

4. DISCUSSION

This work explores the relationship between cloud droplet number concentration and liquid water path using a large-domain large-eddy ICON-LES simulation and MODIS satellite. The satellite retrievals use adiabatic assumptions to retrieve N_{Ad} (adiabatic N_d) from cloud optical depth and effective radius (Quaas et al. 2006). The N_d/N_{Ad} -LWP relationship has the advantage of accounting for the confounding influence of relative humidity, compared to earlier studies that investigated aerosol impacts on LWP by correlating LWP to aerosol optical depth or relative aerosol retrievals (e.g., Nakajima et al., 2001; Sekiguchi et al., 2003; Quaas et al., 2004). However, the model-simulated N_d includes non-adiabatic conditions. Here we have demonstrated the issues in interpreting the satellite-retrieved N_{Ad} -LWP relationships using satellite forward-operator diagnostics (similar to the satellite retrieval, N_{Ad} is derived from the model) by a large-domain large-eddy simulation compared to corresponding satellite observation. Our analysis shows that, when using N_{Ad} in both model and the satellite, the N_{Ad} -LWP relationship is in approximate agreement; a positive N_{Ad} -LWP relationship is observed, especially at higher N_{Ad} ($N_{Ad} > 100 \text{ cm}^{-3}$) with a peak CP confined to the lower N_{Ad} and LWP in both cases. Additionally, for high N_{Ad} , the LWP increases non-linearly with increasing N_{Ad} . However, both the model and the satellite N_{Ad} -LWP relationship lack, in particular, the negative relationship at higher N_{Ad} , reported in previous studies analyzing satellite data over Global Oceans (Gryspeerd et al., 2019).

The model simulation output may be used to test the adiabatic assumption. This is particularly useful since the continental clouds are primarily sub-adiabatic, associated with entrainment and mixing, compared to marine clouds. The LWP increases at lower cloud-top N_d and decreases at higher levels, illustrating cloud lifetime (specifically for non-precipitating clouds) and entrainment effects. However, for the adiabatic cloud regime, in both model and the satellite, a positive N_{Ad} -LWP relationship dominates, with peak CP confined to the lower N_{Ad} and LWP bins of the joint histogram. Additionally, the N_{Ad} -LWP sensitivity is weak at the lower N_{Ad} , but it clearly shows a positive relationship at the higher levels. It implies that both model and the satellite could only explain the precipitation suppression; however, it lacks the entrainment effect on cloud

droplets, which is associated with a negative N_d -LWP relation. A comparison between model-simulated N_d and N_{Ad} illustrates a nonlinear relationship, especially at the lower values. However, a relatively strong correlation is found at the higher N_d/N_{Ad} . It clearly indicates the constraints in the adiabatic assumption in inferring N_{Ad} and the subsequent N_{Ad} -LWP relationship.

Further satellite analysis shows a regime dependency (marine and continental) in the N_{Ad} -LWP relation. The selected single-day limited-area case indeed is representative of NH Land areas in terms of the analyzed relationship. However, Oceanic clouds show nonlinear positive and negative N_{Ad} -LWP relationships at low and high N_{Ad} , respectively, comparable to the previous satellite analysis reported by Gryspeerd et al. (2019), even if a longer period is considered here. A possible explanation for the regime dependency in the N_{Ad} -LWP relation is that the continental clouds can be more associated with sub-adiabatic N_d profiles due to entrainment and mixing than the marine clouds. However, a negative N_{Ad} -LWP relationship is lacking in the continental clouds, which attribute to the constraints in the adiabatic assumption in deriving the N_{Ad} .

Since the ICON-LES simulation is over the continental region and accounts for the regime dependency in the satellite-derived N_{Ad} -LWP relationship, further analysis explored the N_{Ad} -LWP relation in the adiabatic and sub-adiabatic parts of the cloud. Consequently, the regimes-based analysis could overcome the problems in diagnosing the LWP response from such statistical analysis. The model analysis demonstrates that comparatively thin (stratiform) clouds have a rather vertically uniform N_d profile, justifying the adiabatic assumption in the retrievals. However, for deeper clouds, the adiabaticity is violated considering all clouds in the joint histogram. In general, the N_{Ad} is almost always larger than N_d at the cloud-top, leading to differences in the N_d -LWP relationships between thick (convective) and thin (stratiform) clouds and between the relationships considering N_{Ad} and N_d , respectively. A reliable assessment is expected for comparatively thin, stratiform clouds that may be considered an approximately adiabatic cloud regime. In contrast, the convective continental clouds are mostly sub-adiabatic, associated with entrainment and mixing, compared to shallow clouds. In the ICON-LES, the shallow cloud regime shows a positive N_d -LWP sensitivity, similar to the satellite retrievals, while the convective cloud regime shows a nonlinear relationship identical to the entire model analysis over Germany. The diverse N_d/N_{Ad} -LWP relationship in adiabatic and sub-adiabatic cloud regimes further suggests that the regime-based analysis would be more relevant when model simulations are compared with satellite retrievals, especially in the warm continental clouds, which are subjected to more entrainment and mixing compared to the marine clouds.

5. CONCLUSIONS

In the boreal spring (2 May 2013) over Germany, the $N_d(N_{Ad})$ -LWP sensitivity has been explored between the ICON-LES and the satellite retrievals using a joint probability histogram method. Several studies suggest that the satellite inferred N_{Ad} -LWP relationship is consistent with high-resolution model results (Ackerman et al., 2004; Sato et al., 2018). However, this study demonstrated that the satellite-derived N_{Ad} -LWP relationship is inconsistent with the relation predicted by the high-resolution ICON-LES model (N_d -LWP). Conversely, the N_{Ad} -LWP sensitivity is consistent in the model and the satellite analysis. In both cases, the peak CP appears at the lower N_{Ad} values, and the \overline{LWP} increase with the increase in N_{Ad} , particularly above 50 cm^{-3} . While, it lacks the entrainment effect on cloud droplets, associated with the negative N_{Ad} -LWP relationship at higher N_{Ad} . However, the N_d -LWP relationship in the ICON-LES shows a nonlinear relationship with peak CP confined to the \overline{LWP} , especially at the higher levels. The N_d -LWP sensitivity clearly illustrates the cloud lifetime and the entrainment effect. Thus the diverse N_{Ad}/N_d -LWP relation explains the constraints in adiabatic assumption deriving N_{Ad} and the resulting N_{Ad} -LWP relationship that lacks the negative sensitivity or the entrainment effect.

Our analysis suggests that regime-based analysis would be more relevant when comparing the model or observations with the satellite retrievals, especially in the warm continental clouds subjected to entrainment and mixing compared to the marine clouds. In principle, the N_{Ad} represents the adiabatic part of the clouds, which could be considered in both the model simulation and the satellite retrievals when comparing the N_{Ad} -LWP relation. We have demonstrated that, while using N_{Ad} in both model and the satellite, the N_{Ad} -LWP relationship is in approximate agreement. Alternatively, thin shallow clouds with relatively uniform vertical N_d profiles justify the adiabatic assumption, and it also shows a positive N_d -LWP sensitivity, similar to the satellite retrievals. Thus, the statistical relation between the model simulations and the satellite retrievals is comparable when using a consistent assumption. Since the N_d -LWP relationship significantly impacts effective radiative forcing, considering the appropriate cloud regime in the model simulations and its comparisons with the satellite observation would open a new avenue in studying the effect of clouds on climate change.

DATA ACCESSIBILITY STATEMENT

The model output data used for the development of the research in the frame of this scientific article is securely saved in tape archives at the Deutsches Klimarechenzentrum (DKRZ), which will be accessible for

10 years. Additionally, backup copies are stored in the University of Leipzig and University of Cologne backup services. The satellite-based observational data used in the present research are acquired from the Level1 and Atmosphere Archive & Distribution System (LAADS) Distributed Active Archive Center (DAAC), located in the Goddard Space Flight Center in Greenbelt, Maryland (<https://ladsweb.nascom.nasa.gov/>).

ADDITIONAL FILE

The additional file for this article can be found as follows:

- **Figure S1.** The relation between cloud depth (m) and LWP (g m^{-2}) as a function of cloud adiabaticity (α) in the ICON-LES simulation over Germany. DOI: <https://doi.org/10.16993/tellusb.27.s1>

ACKNOWLEDGEMENTS

This study has been carried out under the project “FORCeS”, which is funded by the European Union’s Horizon 2020 research and innovation programme under grant agreement No 821205. Further funding from the DFG-ANR project “CDNC4aci” (Deutsche Forschungsgemeinschaft, DFG GZ QU 311/27-1) is acknowledged. The Co-authors, Annica M. L. Ekman and Matthias Schwarz, also acknowledge the funding of the Swedish Science Foundation (VR) project 2020-04158. We thank the High Definition Clouds and Precipitation for Advancing Climate Prediction (HD(CP)2) project (funded by the German Federal Ministry of Education and Research (BMBF; <http://www.fona.de/>) under grant no. 01LK1504B) for providing the model simulations. EG was supported by a Royal Society University Research Fellowship (URF/R1/191602). We thank the anonymous reviewers for their valuable comments on an earlier version of this manuscript.

COMPETING INTERESTS

The authors declare that they have no conflict of interest. The funders had no role in the design of the study; in the collection, analyses, or interpretation of data; in the writing of the manuscript, or in the decision to publish the results.

AUTHOR CONTRIBUTIONS

All authors participated in the design of the study. DS & JQ conceived and refined the overall structure of the investigation based on discussions with and

feedback from all co-authors. All authors assisted in the interpretation of the results and commented on the paper. All authors have read and agreed to the published version of the manuscript.

AUTHOR AFFILIATIONS

Sudhakar Dipu  orcid.org/0000-0003-4514-8968
Institute for Meteorology, Universität Leipzig, Leipzig, Germany

Matthias Schwarz  orcid.org/0000-0002-0043-3522
Department of Meteorology and Bolin Centre for Climate Research, Stockholm University, Stockholm, Sweden; Now at ZAMG – Zentralanstalt für Meteorologie und Geodynamik, Vienna, Austria

Annica M. L. Ekman  orcid.org/0000-0002-5940-2114
Department of Meteorology and Bolin Centre for Climate Research, Stockholm University, Stockholm, Sweden

Edward Gryspeerdt  orcid.org/0000-0002-3815-4756
Space and Atmospheric Physics Group, Imperial College London, UK

Tom Goren  orcid.org/0000-0001-5618-9402
Institute for Meteorology, Universität Leipzig, Leipzig, Germany

Odran Sourdeval  orcid.org/0000-0002-2822-5303
Laboratoire d'Optique Atmosphérique, Université de Lille, France

Johannes Mülmenstädt  orcid.org/0000-0003-1105-6678
Institute for Meteorology, Universität Leipzig, Leipzig, Germany; Now at Pacific Northwest National Laboratory, Richland, USA

Johannes Quaas  orcid.org/0000-0001-7057-194X
Institute for Meteorology, Universität Leipzig, Leipzig, Germany

REFERENCES

Ackerman, AS, Kirkpatrick, MP, Stevens, DE and Toon, OB.

2004. The impact of humidity above stratiform clouds on indirect aerosol climate forcing. *Nature*, 432(7020): 1014–1017. DOI: <https://doi.org/10.1038/nature03174>

Albrecht, BA. 1989. Aerosols, cloud microphysics, and fractional cloudiness. *Science*, 245(4923): 1227–1230. DOI: <https://doi.org/10.1126/science.245.4923.1227>

Baldauf, M, Seifert, A, Förstner, J, Majewski, D, Raschendorfer, M and Reinhardt, T. 2011. Operational convective-scale numerical weather prediction with the cosmo model: Description and sensitivities. *Mon. Weather Rev.*, 139(12): 3887–3905. DOI: <https://doi.org/10.1175/MWR-D-10-05013.1>

Bellouin, N, Quaas, J, Gryspeerdt, E, Kinne, S, Stier, P, Watson-Parris, D, Boucher, O, Carslaw, K, Christensen, M, Daniau, A-L, Dufresne, J-L, Feingold, G, Fiedler, S, Forster, P, Gettelman, A, Haywood, JM, Lohmann, U, Malavelle, F, Mauritsen, T, McCoy, D, Myhre, G, Mülmenstädt, J, Neubauer, D, Possner, A, Rugenstein, M, Sato, Y, Schulz, M, Schwartz, SE, Sourdeval, O, Storelvmo, T, Toll, V, Winker, D and Stevens, B. 2020. Bounding global aerosol radiative forcing of climate change. *Rev. Geophys.*, 58: e2019RG000660. DOI: <https://doi.org/10.1029/2019RG000660>

Bennartz, R and Rausch, J. 2017. Global and regional estimates of warm cloud droplet number concentration based on 13 years of aqua-modis observations. *Atmos. Chem. Phys.*, 17(16): 9815–9836. DOI: <https://doi.org/10.5194/acp-17-9815-2017>

Braun, RA, Dadashazar, H, MacDonald, AB, Crosbie, E, Jonsson, HH, Woods, RK, Flagan, RC, Seinfeld, JH and Sorooshian, A. 2018. Cloud adiabaticity and its relationship to marine stratocumulus characteristics over the northeast pacific ocean. *J. Geophys. Res. Atmos.*, 123(24): 13,790–13,806. DOI: <https://doi.org/10.1029/2018JD029287>

Brenguier, J-L, Pawlowska, H, Schüller, L, Preusker, R, Fischer, J and Fouquart, Y. 2000. Radiative properties of boundary layer clouds: Droplet effective radius versus number concentration. *J. Atmos. Sci.*, 57(6): 803–821. DOI: [https://doi.org/10.1175/1520-0469\(2000\)057<0803:RPOBLC>2.0.CO;2](https://doi.org/10.1175/1520-0469(2000)057<0803:RPOBLC>2.0.CO;2)

Bulatovic, I, Ekman, AML, Savre, J, Riipinen, I and Leck, C. 2019. Aerosol indirect effects in marine stratocumulus: The importance of explicitly predicting cloud droplet activation. *Geophys. Res. Lett.*, 46(6): 3473–3481. DOI: <https://doi.org/10.1029/2018GL081746>

Charlson, RJ, Schwartz, SE, Hales, JM, Cess, RD, Coakley, JA, Hansen, JE and Hofmann, DJ. 1992. Climate forcing by anthropogenic aerosols. *Science*, 255(5043): 423–430. DOI: <https://doi.org/10.1126/science.255.5043.423>

Chen, Y-C, Christensen, MW, Stephens, GL and Seinfeld, JH. 2014. Satellite-based estimate of global aerosol-cloud radiative forcing by marine warm clouds. *Nat. Geosci.*, 7(9): 643–646. DOI: <https://doi.org/10.1038/ngeo2214>

Christensen, MW, Jones, WK and Stier, P. 2020. Aerosols enhance cloud lifetime and brightness along the stratus-to-cumulus transition. *Proc. Nat. Acad. Sci. USA*, 117b: 17591–17598. DOI: <https://doi.org/10.1073/pnas.1921231117>

Christensen, MW, Neubauer, D, Poulsen, CA, Thomas, GE, McGarragh, GR, Povey, AC, Proud, SR and Grainger, RG. 2017. Unveiling aerosol–cloud interactions – part 1: Cloud contamination in satellite products enhances the aerosol indirect forcing estimate. *Atmos. Chem. Phys.*, 17(21): 13151–13164. DOI: <https://doi.org/10.5194/acp-17-13151-2017>

Costa-Surós, M, Sourdeval, O, Acquistapace, C, Baars, H, Carbajal Henken, C, Genz, C, Hesemann, J, Jimenez, C, König, M, Kretzschmar, J, Madenach, N, Meyer, CI, Schrödner, R, Seifert, P, Senf, F, Brueck, M, Cioni, G, Engels, JF, Fieg, K, Gorges, K, Heinze, R, Siligam, PK, Burkhardt, U, Crewell, S, Hoose, C, Seifert, A, Tegen, I and Quaas, J. 2020. Detection and attribution of aerosol–cloud interactions in large-domain large-eddy simulations with the icosahedral non-hydrostatic model. *Atmos. Chem. Phys.*, 20(9): 5657–5678. DOI: <https://doi.org/10.5194/acp-20-5657-2020>

Dipankar, A, Stevens, B, Heinze, R, Moseley, C, Zügl, G, Giorgetta, M and Brdar, S. 2015. Large eddy simulation

- using the general circulation model icon. *J. Adv. Model. Earth Syst.*, 7(3): 963–986. DOI: <https://doi.org/10.1002/2015MS000431>
- Feingold, G, Eberhard, WL, Veron, DE and Previdi, M.** 2003. First measurements of the twomey indirect effect using ground-based remote sensors. *Geophys. Res. Lett.*, 30(6): DOI: <https://doi.org/10.1029/2002GL016633>
- Forster, P, Storelvmo, T, Armour, K, Collins, W, Dufresne, J-L, Frame, D, Lunt, D, Mauritsen, T, Palmera, M, Watanabea, M, Wild, M and Zhang, H.** 2021. The Earth's Energy Budget, Climate Feedbacks, and Climate Sensitivity. In Masson-Delmotte, V, Zhai, P, Pirani, A, Connors, SL, Péan, C, Berger, S, Caud, N, Chen, Y, Goldfarb, L, Gomis, MI, Huang, M, Leitzell, K, Lonnoy, E, Matthews, JBR, Maycock, TK, Waterfield, T, Yelekçi, O, Yu, R and Zhou, B (eds.), *Climate Change 2021: The Physical Science Basis. Contribution of Working Group I to the Sixth Assessment Report of the Intergovernmental Panel on Climate Change* (Chapter 7). Cambridge University Press. In Press.
- Glassmeier, F, Hoffmann, F, Johnson, JS, Yamaguchi, T, Carslaw, KS and Feingold, G.** 2021. Aerosol-cloud-climate cooling overestimated by ship-track data. *Science*, 371: 485–489. DOI: <https://doi.org/10.1126/science.abd3980>
- Grosvenor, DP, Sourdeval, O, Zuidema, P, Ackerman, A, Alexandrov, MD, Bennartz, R, Boers, R, Cairns, B, Chiu, JC, Christensen, M, Deneke, H, Diamond, M, Feingold, G, Fridlind, A, Hünerbein, A, Knist, C, Kollias, P, Marshak, A, McCoy, D, Merk, D, Painemal, D, Rausch, J, Rosenfeld, D, Russchenberg, H, Seifert, P, Sinclair, K, Stier, P, van Diedenhoven, B, Wendisch, M, Werner, F, Wood, R, Zhang, Z and Quaas, J.** 2018. Remote sensing of droplet number concentration in warm clouds: A review of the current state of knowledge and perspectives. *Rev. Geophys.*, 56(2): 409–453. DOI: <https://doi.org/10.1029/2017RG000593>
- Grosvenor, DP and Wood, R.** 2014. The effect of solar zenith angle on modis cloud optical and microphysical retrievals within marine liquid water clouds. *Atmos. Chem. Phys.*, 14(14): 7291–7321. DOI: <https://doi.org/10.5194/acp-14-7291-2014>
- Gryspeerd, E, Goren, T and Smith, TWP.** 2021. Observing the timescales of aerosol–cloud interactions in snapshot satellite images. *Atmos. Chem. Phys.*, 21: 6093–6109. DOI: <https://doi.org/10.5194/acp-21-6093-2021>
- Gryspeerd, E, Goren, T, Sourdeval, O, Quaas, J, Mülmenstädt, J, Dipu, S, Unglaub, C, Gettelman, A and Christensen, M.** 2019. Constraining the aerosol influence on cloud liquid water path. *Atmos. Chem. Phys.*, 19(8): 5331–5347. DOI: <https://doi.org/10.5194/acp-19-5331-2019>
- Gryspeerd, E, Quaas, J and Bellouin, N.** 2016. Constraining the aerosol influence on cloud fraction. *J. Geophys. Res. Atmos.*, 121(7): 3566–3583. DOI: <https://doi.org/10.1002/2015JD023744>
- Hasekamp, OP, Gryspeerd, E and Quaas, J.** 2019. Analysis of polarimetric satellite measurements suggests stronger cooling due to aerosol-cloud interactions. *Nat. Commun.*, 10(1): 5405. DOI: <https://doi.org/10.1038/s41467-019-13372-2>
- Heiblum, RH, Pinto, L, Altaratz, O, Dagan, G and Koren, I.** 2019. Core and margin in warm convective clouds – part 1: Core types and evolution during a cloud's lifetime. *Atmos. Chem. Phys.*, 19(16): 10717–10738. DOI: <https://doi.org/10.5194/acp-19-10717-2019>
- Heinze, R, Dipankar, A, Henken, CC, Moseley, C, Sourdeval, O, Trömel, S, Xie, X, Adamidis, P, Ament, F, Baars, H, Barthlott, C, Behrendt, A, Blahak, U, Bley, S, Brdar, S, Brueck, M, Crewell, S, Deneke, H, Di Girolamo, P, Evaristo, R, Fischer, J, Frank, C, Friederichs, P, Göcke, T, Gorges, K, Hande, L, Hanke, M, Hansen, A, Hege, H-C, Hoose, C, Jahns, T, Kalthoff, N, Klocke, D, Kneifel, S, Knippertz, P, Kuhn, A, van Laar, T, Macke, A, Maurer, V, Mayer, B, Meyer, CI, Muppa, SK, Neggers, RAJ, Orlandi, E, Pantillon, F, Pospichal, B, Röber, N, Scheck, L, Seifert, A, Seifert, P, Senf, F, Siligam, P, Simmer, C, Steinke, S, Stevens, B, Wapler, K, Weniger, M, Wulfmeyer, V, Zängl, G, Zhang, D and Quaas, J.** 2017. Large-eddy simulations over germany using icon: a comprehensive evaluation. *Q. J. R. Meteorol. Soc.*, 143(702): 69–100. DOI: <https://doi.org/10.1002/qj.2947>
- Jia, H, Ma, X, Yu, F and Quaas, J.** 2021. Significant underestimation of radiative forcing by aerosol–cloud interactions derived from satellite-based methods. *Nat. Commun.*, 12(1): 3649. DOI: <https://doi.org/10.1038/s41467-021-23888-1>
- Koren, I, Dagan, G and Altaratz, O.** 2014. From aerosol-limited to invigoration of warm convective clouds. *Science*, 344(6188): 1143–1146. DOI: <https://doi.org/10.1126/science.1252595>
- Lilly, DK.** 1962. On the numerical simulation of buoyant convection. *Tellus*, 14(2): 148–172. DOI: <https://doi.org/10.1111/j.2153-3490.1962.tb00128.x>
- Löhnert, U, Schween, JH, Acquistapace, C, Ebell, K, Maahn, M, Barrera-Verdejo, M, Hirsikko, A, Bohn, B, Knaps, A, O'Connor, E, Simmer, C, Wahner, A and Crewell, S.** 2015. Joyce: Jülich observatory for cloud evolution. *Bull. Amer. Meteor. Soc.*, 96(7): 1157–1174. DOI: <https://doi.org/10.1175/BAMS-D-14-00105.1>
- Madhavan, BL, Kalisch, J and Macke, A.** 2016. Shortwave surface radiation network for observing small-scale cloud inhomogeneity fields. *Atmos. Meas. Tech.*, 9(3): 1153–1166. DOI: <https://doi.org/10.5194/amt-9-1153-2016>
- McCoy, DT, Bender, FA-M, Mohrmann, JKC, Hartmann, DL, Wood, R and Grosvenor, DP.** 2017. The global aerosol-cloud first indirect effect estimated using modis, merra, and aerocom. *J. Geophys. Res. Atmos.*, 122(3): 1779–1796. DOI: <https://doi.org/10.1002/2016JD026141>
- Menzel, W, Frey, R and Baum, B.** 2015. Terra/modis cloud product 5-min l2 swath 1 km and 5 km, c6, nasa level-1 and atmosphere archive & distribution system (laads) distributed active archive center (daac). Greenbelt, MD: Goddard Space Flight Center. DOI: https://doi.org/10.5067/MODIS/MOD06_L2.006

- Michibata, T, Suzuki, K, Sato, Y and Takemura, T.** 2016. The source of discrepancies in aerosol–cloud–precipitation interactions between gcm and a-train retrievals. *Atmos. Chem. Phys.*, 16(23): 15413–15424. DOI: <https://doi.org/10.5194/acp-16-15413-2016>
- Mülmenstädt, J and Feingold, G.** 2018. The radiative forcing of aerosol–cloud interactions in liquid clouds: Wrestling and embracing uncertainty. *Curr. Clim. Chang. Rep.*, 4(1): 23–40. DOI: <https://doi.org/10.1007/s40641-018-0089-y>
- Nakajima, T, Higurashi, A, Kawamoto, K and Penner, JE.** 2001. A possible correlation between satellite-derived cloud and aerosol microphysical parameters. *Geophys. Res. Lett.*, 28(7): 1171–1174. DOI: <https://doi.org/10.1029/2000GL012186>
- Platnick, S, Meyer, KG, King, MD, Wind, G, Amarasinghe, N, Marchant, B, Arnold, GT, Zhang, Z, Hubanks, PA, Holz, RE, Yang, P, Ridgway, WL and Riedi, J.** 2017. *The modis cloud optical and microphysical products: Collection 6 updates and examples from terra and aqua.* DOI: <https://doi.org/10.1109/TGRS.2016.2610522>
- Quaas, J, Arola, A, Cairns, B, Christensen, M, Deneke, H, Ekman, AML, Feingold, G, Fridlind, A, Gryspeerdt, E, Hasekamp, O, Li, Z, Lipponen, A, Ma, P-L, Mülmenstädt, J, Nenes, A, Penner, JE, Rosenfeld, D, Schrödner, R, Sinclair, K, Sourdeval, O, Stier, P, Tesche, M, van Diedenhoven, B and Wendisch, M.** 2020. Constraining the twomey effect from satellite observations: issues and perspectives. *Atmos. Chem. Phys.*, 20(23): 15079–15099. DOI: <https://doi.org/10.5194/acp-20-15079-2020>
- Quaas, J, Boucher, O, Bellouin, N and Kinne, S.** 2008. Satellite-based estimate of the direct and indirect aerosol climate forcing. *J. Geophys. Res. Atmos.*, 113(D5). DOI: <https://doi.org/10.1029/2007JD008962>
- Quaas, J, Boucher, O and Bréon, F-M.** 2004. Aerosol indirect effects in polder satellite data and the laboratoire de météorologie dynamique–zoom (lmdz) general circulation model. *J. Geophys. Res. Atmos.*, 109(D8). DOI: <https://doi.org/10.1029/2003JD004317>
- Quaas, J, Boucher, O and Lohmann, U.** 2006. Constraining the total aerosol indirect effect in the lmdz and echam4 gcms using modis satellite data. *Atmos. Chem. Phys.*, 6(4): 947–955. DOI: <https://doi.org/10.5194/acp-6-947-2006>
- Ramanathan, V, Cess, RD, Harrison, EF, Minnis, P, Barkstrom, BR, Ahmad, E and Hartmann, D.** 1989. Cloud-radiative forcing and climate: Results from the earth radiation budget experiment. *Science*, 243(4887): 57–63. DOI: <https://doi.org/10.1126/science.243.4887.57>
- Rosenfeld, D, Sherwood, S, Wood, R and Donner, L.** 2014. Climate effects of aerosol–cloud interactions. *Science*, 343(6169): 379–380. DOI: <https://doi.org/10.1126/science.1247490>
- Saponaro, G, Sporre, MK, Neubauer, D, Kokkola, H, Kolmonen, P, Sogacheva, L, Arola, A, de Leeuw, G, Karset, IHH, Laaksonen, A and Lohmann, U.** 2020. Evaluation of aerosol and cloud properties in three climate models using modis observations and its corresponding cosp simulator, as well as their application in aerosol–cloud interactions. *Atmos. Chem. Phys.*, 20(3): 1607–1626. DOI: <https://doi.org/10.5194/acp-20-1607-2020>
- Sato, Y, Goto, D, Michibata, T, Suzuki, K, Takemura, T, Tomita, H and Nakajima, T.** 2018. Aerosol effects on cloud water amounts were successfully simulated by a global cloud-system resolving model. *Nat. Commun.*, 9(1): 985. DOI: <https://doi.org/10.1038/s41467-018-03379-6>
- Schüller, L, Bennartz, R, Fischer, J and Brenguier, J-L.** 2005. An algorithm for the retrieval of droplet number concentration and geometrical thickness of stratiform marine boundary layer clouds applied to modis radiometric observations. *J. Appl. Meteorol.*, 44(1): 28–38. DOI: <https://doi.org/10.1175/JAM-2185.1>
- Seifert, A and Beheng, KD.** 2006. A two-moment cloud microphysics parameterization for mixed-phase clouds. part 1: Model description. *Meteorol. Atmos. Phys.*, 92(1): 45–66. DOI: <https://doi.org/10.1007/s00703-005-0112-4>
- Sekiguchi, M, Nakajima, T, Suzuki, K, Kawamoto, K, Higurashi, A, Rosenfeld, D, Sano, I and Mukai, S.** 2003. A study of the direct and indirect effects of aerosols using global satellite data sets of aerosol and cloud parameters. *J. Geophys. Res. Atmos.*, 108(D22). DOI: <https://doi.org/10.1029/2002JD003359>
- Sommeria, G and Deardorff, J.** 1977. Subgrid-scale condensation in models of nonprecipitating clouds. *J. Atmos. Sci.*, 34: 344–355. DOI: [https://doi.org/10.1175/1520-0469\(1977\)034<0344:SSCIMO>2.0.CO;2](https://doi.org/10.1175/1520-0469(1977)034<0344:SSCIMO>2.0.CO;2)
- Stephens, GL, Christensen, M, Andrews, T, Haywood, J, Malavelle, FF, Suzuki, K, Jing, X, Lebsock, M, Li, J-LF, Takahashi, H and Sy, O.** 2019. Cloud physics from space. *Q. J. R. Meteorol. Soc.*, 145(724): 2854–2875. DOI: <https://doi.org/10.1002/qj.3589>
- Stevens, B and Feingold, G.** 2009. Untangling aerosol effects on clouds and precipitation in a buffered system. *Nature*, 461(7264): 607–613. DOI: <https://doi.org/10.1038/nature08281>
- Suzuki, K, Stephens, GL and Lebsock, MD.** 2013. Aerosol effect on the warm rain formation process: Satellite observations and modeling. *J. Geophys. Res. Atmos.*, 118(1): 170–184. DOI: <https://doi.org/10.1002/jgrd.50043>
- Szopa, S, Naik, V, Adhikary, B, Artaxo, P, Berntsen, T, Collins, W, Fuzzi, S, Gallardo, L, Scharr, AK, Klimont, Z, Liao, H, Unger, N and Zanis, P.** 2021. Short-Lived Climate Forcers. In Masson-Delmotte, V, Zhai, P, Pirani, A, Connors, SL, Péan, C, Berger, S, Caud, N, Chen, Y, Goldfarb, L, Gomis, MI, Huang, M, Leitzell, K, Lonnoy, E, Matthews, JBR, Maycock, TK, Waterfield, T, Yelekçi, O, Yu, R and Zhou, B (eds.), *Climate Change 2021: The Physical Science Basis. Contribution of Working Group I to the Sixth Assessment Report of the Intergovernmental Panel on Climate Change* (Chapter 6). Cambridge University Press. In Press.
- Toll, V, Christensen, M, Quaas, J and Bellouin, N.** 2019. Weak average liquid–cloud–water response to anthropogenic

aerosols. *Nature*, 572: 51–55. DOI: <https://doi.org/10.1038/s41586-019-1423-9>

Twomey, S. 1974. Pollution and the planetary albedo.

Atmos. Environ., 8(12): 1251–1256. DOI: [https://doi.org/10.1016/0004-6981\(74\)90004-3](https://doi.org/10.1016/0004-6981(74)90004-3)

Unglaub, C, Block, K, Mülmenstädt, J, Sourdeval, O and Quaas, J. 2020. A new classification of satellite-derived liquid water cloud regimes at cloud scale. *Atmos. Chem. Phys*, 20(4): 2407–2418. DOI: <https://doi.org/10.5194/acp-20-2407-2020>

Xue, H and Feingold, G. 2006. Large-eddy simulations of trade wind cumuli: Investigation of aerosol indirect effects. *J. Atmos. Sci.*, 63(6): 1605–1622. DOI: <https://doi.org/10.1175/JAS3706.1>

Zängl, G, Reinert, D, Rjodas, P and Baldauf, M. 2015. The icon (icosahedral non-hydrostatic) modelling framework of dwd and mpi-m: Description of the non-hydrostatic dynamical core. *Q. J. R. Meteorol. Soc.*, 141(687): 563–579. DOI: <https://doi.org/10.1002/qj.2378>

TO CITE THIS ARTICLE:

Dipu, S, Schwarz, M, Ekman, AML, Gryspeerdt, E, Goren, T, Sourdeval, O, Mülmenstädt, J and Quaas, J. 2022. Exploring Satellite-Derived Relationships between Cloud Droplet Number Concentration and Liquid Water Path Using a Large-Domain Large-Eddy Simulation. *Tellus B: Chemical and Physical Meteorology*, 74(2022): 176–188. DOI: <https://doi.org/10.16993/tellusb.27>

Submitted: 11 February 2022 **Accepted:** 28 August 2022 **Published:** 16 September 2022

COPYRIGHT:

© 2022 The Author(s). This is an open-access article distributed under the terms of the Creative Commons Attribution 4.0 International License (CC-BY 4.0), which permits unrestricted use, distribution, and reproduction in any medium, provided the original author and source are credited. See <http://creativecommons.org/licenses/by/4.0/>.

Tellus B: Chemical and Physical Meteorology is a peer-reviewed open access journal published by Stockholm University Press.

